Optimization of Argon Plasma Working Pressure through Parallel PIC Simulations for Enhancement of Material Surface Treatment

H. Barati[1], A. Torkaman[1], and M. Fardmanesh[1]

[1] *Department of Electrical Engineering, Sharif University of Technology, Tehran, Iran*

(Received: 17. Nov. 2025, Accepted: 12. Dec. 2025, Published online: 15. Dec. 2025)

In this study, a novel method for simulating plasma dynamics using parallel programming has been developed. The equations based on the Particle-in-Cell (PIC) method were utilized and adapted for this purpose. We used 35 processors from the Sharif High-Performance Computing (HPC) center and divided the plasma volume into 35 parts, with each part's PIC equation solved on a separate processor. Once the computations were completed, the results from all processors were combined to form a complete plasma volume. The simulations revealed that there is an optimal pressure for argon, at which the ion flux onto the electrode surface is maximized. Increasing the absolute value of the electrode potential also increases this flux. Therefore, for a given potential, selecting the optimal pressure is crucial for the most effective surface modification using argon plasma. In this work, for an applied voltage of -500 V, the optimum pressure was 100 mTorr.

(DOI: 10.31281/7mgem433)

baratihadi6@gmail.com, hadi.barati@ee.sharif.edu

I. Introduction

Long-term success of medical implants depends on the integration of implant materials with biological tissues [1, 2]. In this process, surface characteristics of implant materials are quite important since they affect cellular reactions including adhesion, proliferation, and differentiation [2, 3]. Different surface modification methods have been investigated to improve the interaction between biological systems and implant surfaces; plasma surface treatment has emerged as a possible solution [4, 5]. This approach improves biocompatibility by allowing the modification of the implant surface without changing its bulk characteristics [5]. The application of argon plasma treatment has been verified as a great enhancing method for both biological and surface properties of metallic and polymeric biomaterials. Hence, several areas of biocompatibility can be affected by argon plasma treatment.

Studies have shown that the argon plasma treatment processes could enhance the hydrophilicity and wetting of implant materials, specifically for polyimide (PI) [6] and titanium [3]. For example, the surface free energy of PI surfaces nearly doubled with plasma treatment [6]. For collagen-based and poly (lactic-co-glycolic acid) (PLGA) scaffolds, argon plasma treatment decreases hydrophobicity, alters surface chemistry, and allows for partial collagen crosslinking, thereby resulting in diminished protein release and increased scaffold stability—parameters that greatly control bone tissue engineering [7]. Similarly, in situ argon plasma treatment on 3D-printed polylactic acid (PLA) scaffolds has been documented as enhancing surface roughness and adding oxygen-containing functional groups but, in turn, diminishing the water contact angle and enhancing adhesion, proliferation, and viability of human adipose-derived stem cells [8]. In metallic substrates such as nanostructured titanium, argon plasma has been found effective in eliminating carbon contaminants, increasing hydrophilicity, and enhancing protein adsorption and osteoblast adhesion without influencing nanoscale morphology, thereby improving enhanced osseointegration [9]. Overall, these results support the inference that argon plasma at the same time manages surface chemistry and topography but, as such, develops a favorable microenvironment that promotes protein adsorption, cell adhesion, and osteogenic differentiation and thereby boosts the biocompatibility of various different implant materials. Besides chemical functionalization, plasma treatment can also modify the physical attributes of the surface of implants, i.e., geometry and roughness, which in turn regulate cellular activity [4, 10]. Variation of nanoscale topography can alter the adsorption kinetics of proteins and impose cellular orientation, spreading, and differentiation directly [3, 6]. Therefore, quantitative insights into the mechanisms by which plasma-induced changes in morphology contribute to biocompatibility require simulation-based analysis, such as the Particle-in-Cell (PIC) technique, for investigating plasma–surface interactions at the microscopic scale [8, 7].

Although several studies have investigated the effects of argon plasma on biocompatibility, the optimization of its treatment parameters still remains an area of continuous research. An understanding of the interplay between plasma properties such as ion energy, density, and surface interaction and their implications on functionalization can significantly facilitate implant surface property enhancement as well as biological response improvement. In this regard, PIC simulation utilization could provide valuable insight into plasma creation, argon ion and radical kinetics as well as their material surface interaction behavior, thus contributing towards the rationalizing plasma process development towards biocompatibility optimization. Thus, the development of implant surfaces with enhanced biological performance could be greatly advanced by research concentrating on the optimization of argon plasma through PIC simulations.

II. PIC description

In the current research, the PIC method is employed for simulating the plasma particle motions. With this method, the time-evolved population of the plasma ions and electrons hitting the substrate surface can be determined. This value is a key variable in assessing the effectiveness of the surface bombardment by the plasma for the purpose of surface functionalization.

In PIC, the plasma is modeled as a mixture of computational (super) particles, including ion and electron super-particles. A super-particle represents a large number (N_p) of real plasma particles with similar energetic and spatial properties. These super-particles are typically treated as having a finite spatial extent or shape. This finite size is crucial as it models the collective behavior of the N_p real particles, reduces unphysical short-range interactions between individual super-particles, and allows the system to mimic a weakly coupled plasma with a computationally tractable number of super-particles.

Here, a non-collisional partially ionized plasma is considered [11], and thus the super-particle distribution throughout the plasma domain can be determined by solving the governing equation of Maxwell-Vlasov:

$$\frac{\partial \mathrm{F_p}}{\partial \mathrm{t}} + \vec{\mathrm{v}} \cdot \nabla_{\vec{\mathrm{R}}} \mathrm{F_p} + \mathrm{q_p}\left(\vec{\mathrm{E}} + \vec{\mathrm{v}} \times \vec{\mathrm{B}}\right) \cdot \nabla_{\vec{\mathrm{p}}} \mathrm{F_p} = 0 \qquad (1)$$

$F_p(\vec{R},\vec{V},t)$ is the probability density distribution function in phase space for a super-particle (representing species p, such as electrons or ions) with charge q_p and momentum $\vec{p} = m_p\vec{V}$. $\vec{V}$ is the velocity vector of each super-particle. $\vec{E}$ and $\vec{B}$ are the macroscopic electric and magnetic fields.

The distribution function for a single super-particle k located at $\vec{r}_k(t)$ with velocity $\vec{V}_k(t)$ is often represented as [13]

$$F_k(\vec{R},\vec{V},t) = N_p\varphi_x\left(\vec{R}-\vec{R}_k(t)\right)\varphi_v(\vec{V}-\vec{V}_k(t)) \quad (2)$$

where φ_x is a spatial shape function and φ_v is a velocity shape function (typically a Dirac delta function, implying all N_p constituent real particles share the velocity $\vec{V}_k$). The total distribution function for species p is

$$F_p = \sum_k F_k \quad (3)$$

In the PIC approach, the Vlasov equation is not directly solved for F_p. Instead, the trajectories of a large number of super-particles are tracked using the characteristic equations (equations of motion), and these particles serve as sources for Maxwell's equations:

$$\frac{\partial\vec{R}_p}{\partial t} = \vec{V}_p \quad (4)$$

$$\frac{\partial\vec{V}_p}{\partial t} = \frac{q_p}{m_p}\left(\vec{E}_p + \vec{V}_p\times\vec{B}_p\right) \quad (5)$$

Here, $\vec{r}_p$ and $\vec{v}_p$ are the position and velocity of an individual super-particle. $\vec{E}_p$ and $\vec{B}_p$ are the electric and magnetic fields at the super-particle's position $\vec{R}_p$. These fields are not the direct microscopic fields but are interpolated from the macroscopic fields $\vec{E}_g$ and $\vec{B}_g$ calculated on a computational grid.

Maxwell's equations govern the evolution of these macroscopic fields:

$$\nabla_g\times\vec{E} = -\frac{\partial\vec{B}}{\partial t} \quad (6)$$

$$\nabla_g\times\vec{B} = \mu_0\vec{J}_g + \frac{1}{c^2}\frac{\partial\vec{E}}{\partial t} \approx \mu_0\vec{J}_g \quad (7)$$

$$\nabla_g\cdot\vec{E} = \frac{\rho_g}{\varepsilon_0} \quad (8)$$

$$\nabla_g\cdot\vec{B} = 0 \quad (9)$$

The approximation in Eq. (7) implies that the displacement current term ($\frac{1}{c^2}\frac{\partial\vec{E}}{\partial t}$) is neglected, often valid for non-relativistic plasmas or low-frequency phenomena.

For the PIC simulation, the plasma region is discretized into a mesh of computational grid points. At these points, Eqs. (6)–(9) are solved. The subscript "g" on operators indicates differentiation performed at the grid points.

The source terms ρ_g (charge density) and $\vec{J}_g$ (current density) are calculated by summing contributions from all super-particles onto the grid. The contribution of each super-particle to the grid-based densities is determined using a weighting or shape function. This function depends on the relative distance between the grid point position $\vec{R}_g$ and the super-particle position $\vec{R}_p$. In this research, the spatial shape of a super-particle itself is conceptually based on the zero-order b-spline function (a rectangular or "top-hat" profile in each dimension):

$$\emptyset_0(\vec{R}_g-\vec{R}_p) = \prod_{i\in\{x,y,z\}}\begin{cases}1\ if\ \frac{|\vec{R}_{g,i}-\vec{R}_{p,i}|}{\|\Delta\vec{R}_i\|} < 0.5\\ 0 Otherwise\end{cases} \quad (10)$$

where ΔR_i is the grid cell size in the dimension i. This b_0 function defines the "cloud" of a super-particle. More generally, for a 1D coordinate ξ, $\emptyset_0(\xi) = 1$ if $\frac{|\xi|}{\Delta\xi} < 0.5$ and 0 otherwise.

The current density $\vec{J}_g$ and charge density ρ_g at a grid point $\vec{R}_g$ are calculated by summing the contributions of all N super-particles, weighted by an interpolation function W:

$$\vec{J}_g(\vec{R}_g) = V_g^{-1}\sum_{k=1}^{N} q_k\vec{V}_k\Delta(\vec{R}_g-\vec{R}_k) \quad (11)$$

$$\rho_g(\vec{R}_g) = V_g^{-1}\sum_{k=1}^{N} q_k\Delta(\vec{R}_g-\vec{R}_k) \quad (12)$$

V_g is the control volume (cell volume) associated with the grid point. q_k(Same as q_i) and $\vec{V}_k$ (same as $\vec{V}_i$) are the charge and velocity of the k^{th} super-particle.

The interpolation function $\Delta(\vec{R}_g-\vec{R}_k)$ determines how a particle's charge and current are distributed to nearby grid points. It is related to the particle shape function. For a $\emptyset_0$ (0th-order b-spline)

particle shape, the commonly used Cloud-In-Cell (CIC) method employs a weighting function W that is a 1st-order b-spline, $\emptyset_1$. This b_1 function can be obtained by convolving two $\emptyset_0$ functions:

$$\Delta(\vec{R}_g - \vec{R}_k) = \emptyset_1(\vec{R}_g - \vec{R}_k) =$$

$$= \int_{-\infty}^{\infty} d\vec{r'}\, \emptyset_0(\vec{R}_g - \vec{R}_k - \vec{r'})\emptyset_0(\vec{r'}) \qquad (13)$$

In multiple dimensions, Δ is typically a product of 1D b_1 functions, e.g.,

$$\Delta(\vec{R}_g - \vec{R}_p) = \emptyset_1\left(\frac{x_g - x_p}{\Delta x}\right)\emptyset_1\left(\frac{y_g - y_p}{\Delta y}\right)\emptyset_1\left(\frac{z_g - z_p}{\Delta z}\right) \qquad (14)$$

This weighting scheme ensures that $\sum_g \Delta(\vec{R}_g - \vec{R}_k) = 1$ for any $\vec{R}_p$. The fields $\vec{E}_p$ and $\vec{B}_p$ acting on a super-particle are obtained by interpolating the grid-based fields $\vec{E}_g, \vec{B}_g$ to the particle's position $\vec{R}_p$.

In the present work, the bombardment of a material surface by plasma particles is investigated. Since the electrode shape of the experimental apparatus is disk-shaped (schematic in Fig. 1), the cylindrical coordinate system (r, θ, z) is chosen for expanding and solving the governing equations. Hence, it is assumed that the plasma is generated inside a cylindrical vacuum chamber and over a DC-powered electrode. The initial pressure of the working gas, i.e., argon is assumed as the working pressure of the plasma.

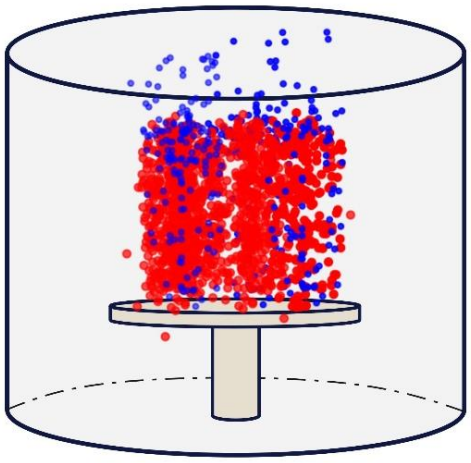

Figure1: Cylindrical vacuum chamber. The plasma is formed over the electrode. The plasma ions and electrons are shown in red and blue, respectively.

For the field solution step, particularly for the electric field which often dominates low-temperature plasma-surface interactions, and when boundary conditions are defined by electrode potentials, it is practical to solve Poisson's equations $\vec{\nabla}^2\Phi = -\frac{\rho_g}{\varepsilon_0}$to find the distribution of electric potential Φ throughout the plasma domain. (Laplace's equation $\vec{\nabla}^2\Phi = 0$ is a special case for $\rho_g = 0$). In cylindrical coordinates:

$$\vec{\nabla}^2\Phi = \frac{1}{r}\frac{\partial}{\partial r}\left(r\frac{\partial\Phi}{\partial r}\right) + \frac{1}{r^2}\frac{\partial^2}{\partial\theta^2}(\Phi) + \frac{\partial^2}{\partial z^2}(\Phi) = -\frac{\rho_g}{\varepsilon_0} \qquad (15)$$

After solving for Φ on the grid, the electric field components are found by $\vec{E}_g = -\nabla_g\Phi$.In the PIC method, numerical stability and accuracy are paramount. This means selecting a time step in a way that satisfies stability criteria (e.g., Courant-Friedrichs-Lewy condition to resolve plasma/cyclotron frequencies [13]), choosing a sufficient number of super-particles per cell to minimize statistical noise, and selecting accurate, conservative interpolation schemes. Boundary conditions for both particles and fields should be handled with utmost care. Traditionally, for simplicity, PIC methods consider super-particles of fixed shape. Strictly speaking, the phase-space volume of an individual super-particle element cannot be conserved as required by Liouville's theorem for the element itself, even though the system as a whole strives to satisfy it.

III. Multi-process (parallel) computation

For the simulations in the present work, we utilized the Sharif University HPC (High Performance Computing) system. In an HPC approach, computations are performed in a parallel manner, requiring the computation code to follow a parallel multi-process programming method. To achieve this, we developed a novel parallel programming method to compute the evolution of plasma particle motions using multiple cores or processes. As shown in Fig. 2, the plasma column is divided into n sectors, where n represents the number of cores or processors available in the HPC system. In this work, we used 35 cores or processes (n=35) from the HPC for the simulations, while for illustration purposes, the plasma column is divided into 10 sectors in Fig. 2. Since each sector is simulated on individual cores or processors, the marginal plasma particles cannot influence each

other directly. To address this issue, the sectors are marginally overlapped, allowing marginal particles to exert force on each other and improving the consistency of the simulation results with plasma dynamics. However, this approach considers the marginal effects twice. To alleviate this problem, the average position and velocity of a marginal particle are taken into account.

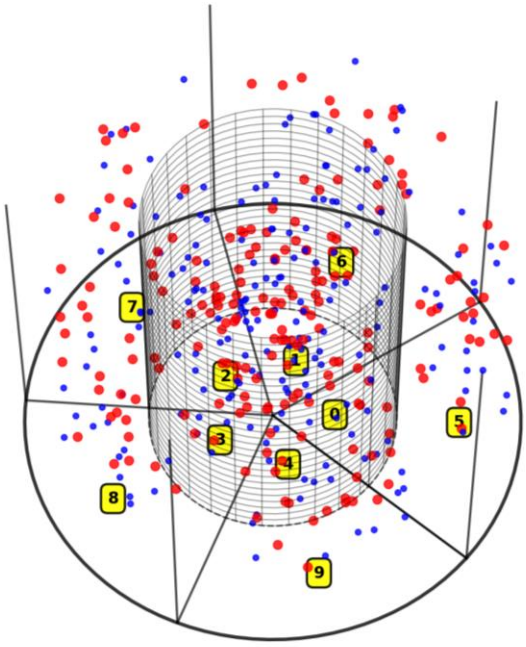

Figure 2: The plasma column is divided to n sectors, for example n=10. The motion evolution of plasma particles located in each sector is simulated on a different core (processor).

IV. Results and discussion

The effects of the working pressure of the argon plasma and the electrode voltage have been investigated through multi-processing simulations. These effects on the ion beam flux impinging on the electrode surface are shown in Figs. 3 and 4, respectively. The amount of pressure influence on the mass and charge of super-particles can be determined through the following equations [12].

$$m_{si} = \frac{V_{plasma}\rho_{Ar,0}}{N_i} P_{Ar} \quad (16)$$

$$m_{se} = \frac{m_e V_{plasma}\rho_{Ar,0}}{M_{Ar}N_i} P_{Ar} \quad (17)$$

$$q_{si} = \frac{Z_{eff} eV_{plasma}\rho_{Ar,0}}{M_{Ar}N_i} P_{Ar} \quad (18)$$

$$q_{se} = \frac{eV_{plasma}\rho_{Ar,0}}{M_{Ar}N_i} P_{Ar} \quad (19)$$

m_{si} and m_{se} are the super-ion and super-electron masses, respectively. $\rho_{Ar,0}$ is the argon mass density at 1 atmosphere pressure. P_{Ar} is the relative filling pressure of argon with respect to 1 atmosphere pressure. V_{plasma} is the argon plasma volume. M_{Ar} is the argon atomic mass. N_i is the number of super-ions that is set manually. The maximum value of N_i is restricted by the HPC computational limitations. Due to Sharif HPC available computational resources, the maximum value of N_i was set equal to 10000. Thus, for partially ionized argon plasma with effective charge number Z_{eff} equal to 11 [12], the number of super-electrons becomes 110000. For the simulations, the electrode potential has been set as various dc values. Thus, the super-ions are attracted by the electrode while the super-electrons are repelled.

The code computes the time-resolved, two-dimensional spatial distribution of ion beam flux incident on the electrode surface. This detailed 2D dataset is spatially averaged across the entire electrode area to generate a one-dimensional temporal profile of the average flux. In Figs. 3 and 4, the dashed red lines indicate the temporal average of this spatially-averaged flux. We consider this value—the time-mean of the area-averaged flux—to be a more comprehensive metric than a single maximum, as it characterizes the steady-state operational flux experienced by the electrode as a whole. The numerical value of this temporal mean is explicitly displayed as a label adjacent to the dashed line. As seen in Fig. 3, the plasma ions exhibit a maximum average hitting-electrode flux of 1.4309×10^{15} (#/m^2 s^{-1}) at a pressure of 100 mTorr compared to pressures of 1, 10, and 200 mTorr. Thus, this pressure can be considered as the optimum working pressure at the electrode potential of -500 V for using argon plasma for material surface functionalization. The average flux at pressures of 1, 10, and 200 mTorr are 1.2936×10^{15}, 1.4293×10^{15}, and 1.3210×10^{15} (#/m^2 s^{-1}), respectively. For investigating the electrode potential's effect on the ion flux bombarding the electrode surface, the working pressure is set at 100 mTorr and simulations are performed for various values of electrode potentials.

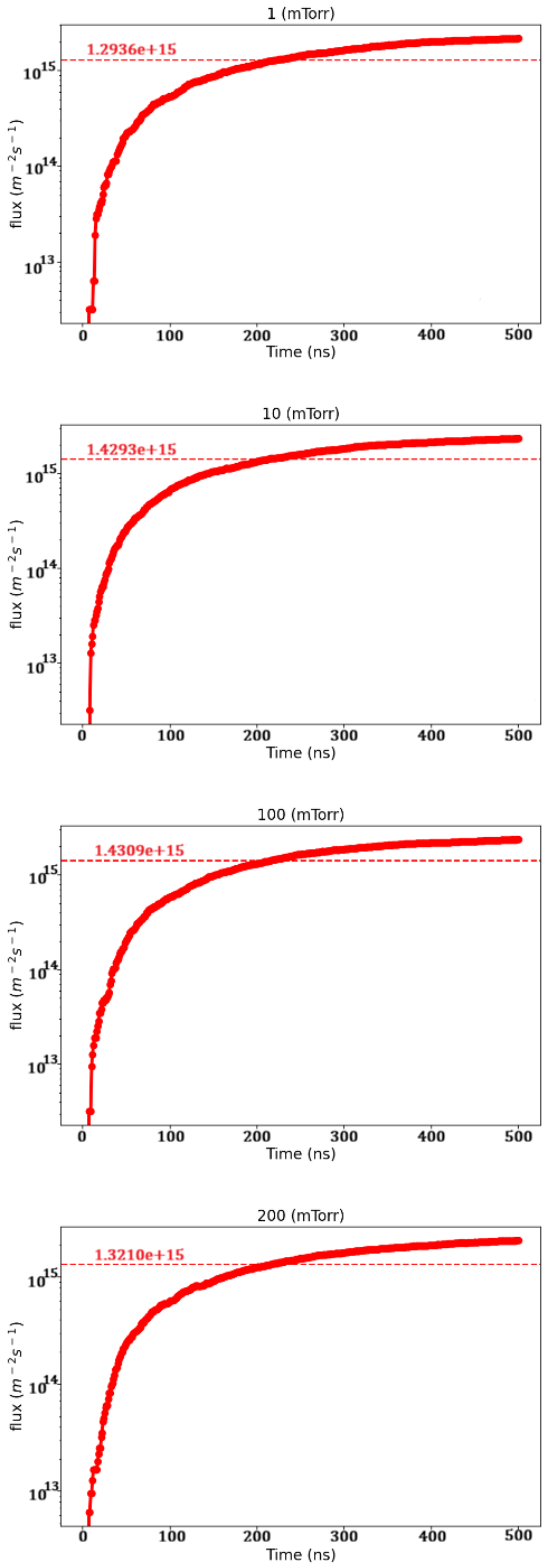

Figure 3: Effect of pressure on ion flux receiving on the electrode surface. The pressure value is shown in title of each case (V=-500 V).

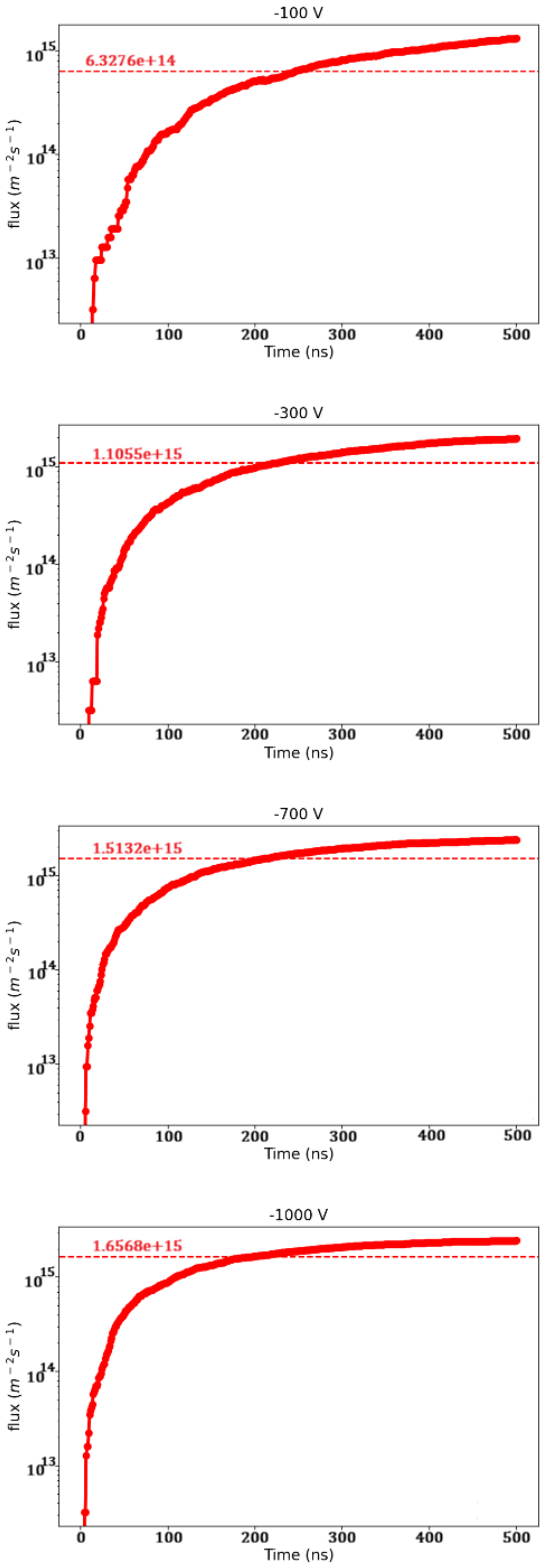

Figure 4: Effect of electrode voltage on ion-flux receiving on the electrode surface. The potential value is shown in title of each case (P=100 mTorr).

The obtained results are illustrated in Fig. 4. As observed, with a more negative potential, a higher flux is obtained. The average flux values are 6.327 x10^{14}, 1.1055 x10^{15}, 1.4309x10^{15} (Fig.3), 1.5132x10^{15}, and 1.6568x10^{15} (#/m^2 s^{-1}) for -100, -300, -500, -700, and -1000 V, respectively. For investigating the effect of electrode potential on the ion flux bombarding the electrode surface, the working pressure is set at 100 mTorr, and simulations are performed for various values of electrode potentials. The results obtained are illustrated in Fig. 4. As observed, with a more negative potential, a higher flux is obtained. The average flux values are 6.327 x 10^{14}, 1.1055 x 10^{15}, 1.4309 x 10^{15} (Fig. 3), 1.5132 x 10^{15}, and 1.6568 x 10^{15} (#/m^2 s^{-1}) for -100, -300, -500, -700, and -1000 V, respectively.

V. Conclusion

In this work, a novel approach for simulating plasma dynamics using parallel programming methods has been developed. The PIC-based Eqs. have been considered and developed for this purpose. We utilized 35 processors from Sharif HPC and divided the plasma volume into 35 parts, with each part's PIC Eq. numerically solved on a different processor. After the computations were completed, the results from all cores were assembled into one plasma volume. The simulations revealed that there is an optimal value for argon pressure at which the ion flux into the electrode surface is maximized. Increasing the absolute value of the electrode potential also increases this flux. Therefore, for a given potential, the optimum pressure should be selected for the most effective surface modification by argon plasma.

VI. References

[1] M. Jasmine Crena, K. Sanjeev, and A. Agarwal. “Plasma treatment as a surface additive for improved hydrophilicity on titanium dental implant surfaces. A systematic review”. *Int. J. Orofac. Biol.*, 8(1), 2024. https://doi.org/10.56501/intjorofacbiol.v8i1.1100

[2] D. Ujino, H. Nishizaki, S. Higuchi, S. Komasa, and J. Okazaki. “Effect of plasma treatment of titanium surface on biocompatibility”. *Appl. Sci.*, 9, 2019. https://doi.org/10.3390/app9112257

[3] R. Hayashi, et al. “Effects of argon gas plasma treatment on biocompatibility of nanostructured titanium”. *Int. J. Mol. Sci.*, 24, 2023. https://doi.org/10.3390/ijms25010149

[4] N. Recek. “Biocompatibility of plasma-treated polymeric implants”. *Materials*, 12, 2019. https://doi.org/10.3390/ma12020240

[5] E. Vassallo, et al. "Plasma treatment of different biodegradable polymers: a method to enhance wettability and adhesion properties for use in industrial packaging." *Plasma,* 7.1 (2024): 91-105. https://doi.org/10.3390/plasma7010007

[6] M. R. Vasquez Jr, E. I. Prieto, and M. Wada, (2018). “Radio-frequency plasma-induced biocompatibility of polyimide substrates”. *Plasma Med.*, *8*(1). https://doi.org/10.1615/PlasmaMed.2018023951

[7] P. T. Vu, J. P. Conroy, and A. M. Yousefi. “The effect of argon plasma surface treatment on poly (lactic-co-glycolic acid)/collagen-based biomaterials for bone tissue engineering”. *Biomimetics*, 7(4), 2022. https://doi.org/10.3390/biomimetics7040218

[8] M. Zarei, S. S. Sayedain, A. Askarinya, M. Sabbaghi, and R. Alizadeh. “Improving physio-mechanical and biological properties of 3d-printed PLA scaffolds via in-situ argon cold plasma treatment”. *Sci. Rep.*, 13, 2023. https://doi.org/10.1038/s41598-023-41226-x

[9] K. Hayashi, et al. “Effects of argon gas plasma treatment on biocompatibility of nanostructured titanium surfaces”. *Int. J. Mol. Sci.*, 25(3), 2024.

[10] N. Gomathi, D. Mishra, T. K. Maiti, and S. Neogi. “Helium plasma treatment to improve biocompatibility and blood compatibility of polycarbonate”. *Surf. Interf. Aspects Cell Adhes.*, 2010. https://doi.org/10.1163/016942410X511088

[11] H. Barati, and M. Habibi. “Calculation of electron beam emitted from argon plasma pinch using the nonrelativistic Vlasov–Maxwell equations”. *IEEE Trans. Plasma Sci.*, 48(11), pp.3862–3870. 2020. https://doi.org/10.1109/TPS.2020.3026451

[12] H. Barati, “Simulation of electron beam emission in Argon–Neon mixture pinch using the nonrelativistic 6-D Valsov–Maxwell system solved by the forward semi-Lagrangian approach”. *IEEE*

Trans. Plasma Sci., 49(3), pp.1142–1151. 2021. https://doi.org/10.1109/TPS.2021.3060479

[13] G. Colonna, and A. D'Angola. "Plasma modeling: Methods and applications". IOP Publishing. In Chapter 4: Particle-based simulation of plasmas. 2022. Online ISBN: 978-0-7503-3559-1, Print ISBN: 978-0-7503-3557-7